Proof-of-concept preparation and characterization of dual-drug amorphous nanoparticle complex as fixed-dose combination of poorly soluble drugs

Yu, Hong; Lim, Li Ming; Dong, Bingxue; Hadinoto, Kunn

2019

Yu, H., Lim, L. M., Dong, B. & Hadinoto, K. (2019). Proof-of-concept preparation and characterization of dual-drug amorphous nanoparticle complex as fixed-dose combination of poorly soluble drugs. Drug Development and Industrial Pharmacy, 45(1), 105-116. https://dx.doi.org/10.1080/03639045.2018.1522327

https://hdl.handle.net/10356/141828

https://doi.org/10.1080/03639045.2018.1522327

Proof-of-Concept Preparation and Characterization of Dual-Drug Amorphous Nanoparticle Complex as Fixed-Dose Combination of Poorly Soluble Drugs

Hong Yu^, Li Ming Lim^, Bingxue Dong, Kunn Hadinoto*

School of Chemical and Biomedical Engineering, Nanyang Technological University, Singapore 637459

^These authors contributed equally to the work

*To whom correspondence should be addressed:

Tel.: (65) 6514 8381, Fax: (65) 6794 7553, E-mail: kunnong@ntu.edu.sg

Statement of novelty: fixed-dose combination of amorphous drug nanoparticle system was developed for the first time in the form of dual-drug amorphous nanoparticle complex exhibiting highly distinct dissolution characteristics from the binary mixture of the single-drug nanoparticle complex

Word counts: 7023

Abstract

Objectives: To carry out a proof-of-concept study on the development of dual-drug amorphous nanoparticle complex (nanoplex in short) as a potential formulation platform for fixed-dose combination (FDC) of poorly-soluble drugs. **Significance**: FDC has been proven effective in improving patient compliance for treatment that requires complex multidrug regimen. Currently, there is growing interest to develop FDC of poorly-soluble drugs due to the increased number of drugs exhibiting poor solubility thus low bioavailability. **Methods**: The dual-drug nanoplex was prepared by electrostatically-driven co-complexation of drug molecules with oppositely charged dextran sulfate, using ciprofloxacin (CIP) and itraconazole (ITZ) as the model poorly-soluble drugs. **Results**: We first verified that the co-complexation products were dual-drug CIP-ITZ nanoplex, and not binary mixtures of the single-drug CIP and ITZ nanoplexes, by demonstrating their distinct thermal behaviors and dissolution characteristics. Depending on the preparation condition, the dual-drug nanoplex exhibited size and zeta potential of 160-410 nm and -35-50 mV, respectively. The individual drug payloads were readily manipulated by varying the CIP/ITZ mass ratio in the feed, resulting in CIP and ITZ payloads in the range of 60-30% and 15-45%, respectively. The CIP-ITZ nanoplex, however, exhibited diminished CIP supersaturation generation, thus lower CIP solubility enhancement, compared to the single-drug CIP nanoplex. The CIP-ITZ nanoplex, nonetheless, remained capable of generating high ITZ supersaturation level. **Conclusion**: Dual-drug nanoplex was successfully prepared with high degree of control over its physical characteristics. Nevertheless, whether dual-drug nanoplex always exhibits diminished solubility enhancement compared to its single-drug counterparts needs to be investigated using different poorly-soluble drugs.

Keywords: nanoparticles; amorphization; fixed dose combination; poorly soluble drugs; complexation

List of abbreviations

AA	acetic acid
ASD	amorphous solid dispersion
C	supersaturated drug concentration
C_{Sat}	drug saturation solubility
CAM	co-amorphous system
CE	complexation efficiency
CIP	ciprofloxacin
COPD	chronic obstructive pulmonary diseases
DTA	differential thermal analysis
DLS	dynamic light scattering
DXT	dextran sulfate
FDC	fixed dose combination
FESEM	field emission scanning electron microscope
FTIR	Fourier transform infrared spectroscopy
HPLC	high performance liquid chromatography
HPMC	hydroxypropylmethylcellulose
ITZ	itraconazole
$M_{ITZ/CIP}$	Mass ratio of ITZ to CIP in the feed solution
MW	molecular weight
PDI	polydispersity index
PXRD	powder x-ray diffraction
$R_{drugs/DXT}$	charge ratio of drug to DXT
SDS	sodium dodecyl sulfate
TGA	thermal gravimetric analysis

1. Introduction

A significant number of common chronic clinical conditions (e.g. hypertension, diabetes, chronic obstructive pulmonary diseases (COPD), arthritis) require treatments involving multiple drugs delivered simultaneously in complex regimens, resulting in low patient compliance [1]. Fixed-dose combination (FDC) drugs in which two or more drugs are formulated in a single oral dosage form have been shown to greatly improve patient compliance compared to a multi-pill regimen [2, 3], while exhibiting similar therapeutic efficacies and safety profiles in the treatment of common chronic diseases [4, 5, 6, 7, 8].

Recently, there is a growing interest to develop FDC formulations of poorly soluble drugs as a large majority of new drug entities possess low aqueous solubility due to their increasingly complex chemistry [9]. Thus far, the research efforts on developing FDC of poorly soluble drugs have focused on amorphous solid dispersion (ASD) and drug-drug co-amorphous systems (CAM) [10, 11, 12, 13, 14]. The reason is because amorphization has been established as one of the most effective drug solubility enhancement strategies [15, 16], which is attributed to the generation of supersaturated drug concentration by the metastable state of the amorphous form, resulting in high apparent solubility [17].

Besides ASD and CAM, a combined amorphization and nanonization approach in the form of amorphous drug nanoparticles have also emerged as an effective solubility enhancement strategy [18]. In fact, amorphous nanoparticles have been shown to be superior to the conventional ASD, albeit for a limited number of drugs, owed to the faster dissolution rates afforded by the large specific surface areas of the nanoparticles [19, 20, 21, 22]. The faster dissolution rates reduce the time-window for solution-mediated crystallization of the amorphous solid phase by Ostwald ripening, resulting in higher supersaturation generation by amorphous drug nanoparticles [23].

To the best of our knowledge, FDC of amorphous drug nanoparticles in which multiple drugs are incorporated in their amorphous states into a single nanoparticle has not been studied before. In fact, the closest work to the development of FDC involving drug nanoparticles was the work by Arora, Shafiq [24] in which three different nanoparticles which each of them encapsulated a different drug were delivered simultaneously to achieve synergistic antihypertension therapy. On this note, while the incorporation of multiple drugs into a single nanoparticle carrier (e.g. lipids, polymers, proteins) by either encapsulation or conjugation has been investigated previously [25, 26],

these nanoparticles were not intended as a solubility enhancement strategy, hence they lacked the supersaturation generation capability exhibited by amorphous drug nanoparticles.

Amorphous drug nanoparticles are typically prepared by either top-down (e.g. wet milling, high pressure homogenization) or bottom-up (e.g. antisolvent precipitation, drug-polyelectrolyte complexation) techniques [18]. Among these techniques, the drug-polyelectrolyte complexation has been deemed most promising because of its (1) ease-of-preparation, (2) high drug utilization rate, and (3) cost effectiveness with minimal energy requirement [27]. In this technique, soluble drug-polyelectrolyte complex is spontaneously formed via electrostatically driven complexation between ionized drug molecules and oppositely charged polyelectrolytes. The soluble complex subsequently form aggregates owed to inter-drug hydrophobic interactions after which they precipitate upon reaching a critical mass, resulting in the formation of amorphous drug-polyelectrolyte nanoparticle complex (or nanoplex in short) [27].

A wide range of poorly soluble drugs have been successfully formulated to form a single-drug amorphous nanoplex exhibiting good solubility enhancement capability [27, 28, 29, 30, 31, 32, 33]. In fact, using itraconazole as the model drug, the amorphous nanoplex has been shown to exhibit superior solubility enhancement to amorphous nanoparticles prepared by antisolvent precipitation [29].

Recognizing the attractive characteristics exhibited by the amorphous nanoplex, the present work aimed to develop a dual-drug amorphous nanoplex intended as a potential FDC platform for poorly soluble drugs. The study was performed using two model drugs that had been successfully transformed into a single-drug amorphous nanoplex in our previous studies, i.e. antibiotic ciprofloxacin (CIP) and antifungal itraconazole (ITZ), with dextran sulfate (DXT) as the polyelectrolytes [27, 29]. Co-deliveries of CIP and ITZ, as well as co-deliveries of CIP or ITZ with other drugs, have been investigated previously [34, 35, 36], therefore demonstrating the potential clinical needs for their FDC formulations.

As illustrated in Fig. 1, the dual-drug nanoplex was herein defined as a nanoplex that was made up of soluble complexes formed by binding between two distinct drug molecules and the polyelectrolyte chains (i.e. CIP-ITZ-DXT complex). Hence, the dual-drug nanoplex was distinguished from a binary mixture of two single-drug nanoplexes that were made up of CIP-DXT and ITZ-DXT complexes. The first objective of the present work was to investigate the feasibility of forming the dual-drug CIP-ITZ nanoplex via co-complexation of cationic CIP and ITZ

with oppositely charged DXT. We aimed to answer the research question "did co-complexation of CIP and ITZ with DXT lead to the formation of dual-drug CIP-ITZ nanoplex or binary mixture of single-drug CIP and ITZ nanoplexes?"

The results showed that the dual-drug CIP-ITZ nanoplex was successfully produced by the co-complexation process with distinct dissolution characteristics and thermal behavior compared to the binary mixture of single-drug nanoplexes. Based on this positive outcome, the second objective of the present work was to subsequently investigate (1) the effect of the preparation condition on the physical characteristics (i.e. size, zeta potential, drug payload) and preparation efficiency (i.e. drug utilization rate, yield) of the CIP-ITZ nanoplex, and (2) whether the individual drug payload in the dual-drug nanoplex could be readily manipulated to obtain the desired therapeutic dosage. Lastly, we examined the effect of having binary drugs on the supersaturation generation capability of the amorphous drug nanoplex.

2. Materials and Methods

2.1. Materials

CIP (≥ 98.0%), glacial acetic acid (AA), hydrogen chloride (HCl), potassium hydroxide (KOH), sodium dodecyl sulfate (SDS), sodium chloride (NaCl), methanol, acetonitrile, potassium dihydrogen phosphate (KH_2PO_4), and hydroxypropylmethylcellulose (HPMC, MW = 86 kDa) were purchased from Sigma-Aldrich (Singapore). ITZ (≥ 98.0%) and DXT (MW = 5 kDa) were purchased from Alfa Aesar (USA) and Wako Pure Chemical (Japan), respectively.

2.2. Methods

2.2.1. Preparation of the dual-drug CIP-ITZ nanoplex

CIP having pK_a of 6.1 and 8.6 and ITZ having pK_a of 3.7 were co-dissolved at 5 mg/mL each in aqueous AA solution at AA = 50% (pH 1.30), 60% (pH 1.17), 70% (pH 0.75), and 80% (pH 0.10) (v/v), resulting in the formation of cationic CIP and ITZ with charge densities of 3.0×10^{-6} and 2.8×10^{-6} mol charge/mg, respectively [27, 29]. DXT with $pK_a \leq 2$ was dissolved separately at 7.3 mg/mL in deionized water (pH ≈ 7) to form anionic DXT with charge density of 4.8×10^{-6} mol charge/mg [27]. These CIP, ITZ, and DXT concentration values corresponded to a charge ratio of drugs to DXT ($R_{drugs/DXT}$) equal to ≈ 0.83. The sample calculations for the charge densities and $R_{drugs/DXT}$ were provided in the Supplementary Materials.

Next, the ionized (CIP+ITZ) and DXT solutions were mixed at equal volumes under vortexing for 10 s, resulting in a mixed (CIP+ITZ+DXT) solution. The resultant CIP-ITZ nanoplex suspension then underwent two cycles of centrifugation (14,000×g for 10 min) and washing with deionized water to remove the excess drugs and DXT that did not form the nanoplex. Afterwards, the washed CIP-ITZ nanoplex was re-suspended in deionized water for characterizations. A control experiment in which the dual-drug solution was mixed with deionized water without DXT at equal volumes was also carried out. The effects of the mass ratio of ITZ to CIP in the feed solution ($M_{ITZ/CIP}$) were investigated by varying the ITZ concentration between 1 and 8 mg/mL at a fixed CIP concentration (i.e. 5 mg/mL), resulting in $0.2 \leq M_{ITZ/CIP} \leq 1.6$.

2.2.2. Physical characterizations of the dual-drug CIP-ITZ nanoplex

The size, zeta potential, and polydispersity index (PDI) of the CIP-ITZ nanoplex were characterized from a minimum of six independent replicates by dynamic light scattering (DLS) after 100× dilution, using Brookhaven 90 Plus Nanoparticle Size Analyzer (Brookhaven Instruments Corporation, USA). The size was verified by field emission scanning electron microscope (FESEM) (JSM 6700F, JEOL, USA) using freeze-dried nanoplex suspension as the sample. The existence of both CIP and ITZ in the dual-drug nanoplex was verified by Fourier transform infrared spectroscopy (FTIR) using Spectrum One FT-IR Spectrometer (Perkin-Elmer, USA) performed between 500 and 4000 cm^{-1} at 1 cm^{-1} spectral resolution. The FTIR analysis was also performed for the native CIP, native ITZ, DXT, CIP nanoplex, and ITZ nanoplex.

The drug payload defined as the amount of drug per unit mass of the nanoplex was determined in triplicates by dissolving a known mass of freeze-dried CIP-ITZ nanoplex in 50% (v/v) aqueous AA solution. Afterwards, the amounts of CIP and ITZ in the solution were determined by high performance liquid chromatography (HPLC) at detection wavelength of 262 nm. The HPLC was carried out in Agilent 1100 (Agilent Technologies, Singapore) using ZORBAX Eclipse Plus C18 column (250×4.6 mm and 5-µm particle size). A mixed solution of acetonitrile and 2 mM KH_2PO_4 (80:20 v/v) adjusted to pH 3.2 by adding AA was used as the mobile phase at flow rate of 1 mL/min. This resulted in the retention time of CIP and ITZ at approximately 2-3 min and 5-6 min, respectively. The total drug payload was calculated from the sum of the CIP payload and ITZ payload.

The amorphous state of the CIP-ITZ nanoplex was verified by powder x-ray diffraction (PXRD) performed between 10° and 70° (2θ) with a step size of 0.02°/s using D8 Advance X-ray Diffractometer (Bruker, Germany).

The thermal behavior of the nanoplex was examined by thermogravimetric analysis (TGA)/ differential thermal analysis (DTA) using Pyris Diamond TG/DTA (Perkin-Elmer, USA) at heating rate of 10°C/min in the range of 25°C to 400°C. Freeze-dried nanoplex powders were used for the PXRD and TGA/DTA analysis. The PXRD and TGA/DTA analysis were also performed for the native CIP, native ITZ, DXT, CIP nanoplex, ITZ nanoplex, and binary mixtures of the CIP and ITZ nanoplexes.

2.2.3. Preparation efficiency of the dual-drug CIP-ITZ nanoplex

The preparation efficiency of the dual-drug nanoplex was reported in terms of the drug utilization rate and overall production yield from a minimum of six independent replicates. The drug utilization rate was characterized by the complexation efficiencies (CE) of CIP and ITZ each defined in Eq. (1) and (2), respectively. The mass of CIP (or ITZ) that formed the CIP-ITZ nanoplex was determined from the difference between the initial mass of CIP (or ITZ) added and the mass of CIP (or ITZ) recovered in the supernatant after first centrifugation of the nanoplex suspension. The amount of CIP (or ITZ) in the supernatant was then determined by HPLC as previously described. The overall production yield was determined in triplicates using Eq. (3), where the mass of CIP-ITZ nanoplex produced was determined from the dry mass of the washed nanoplex suspension after 24-h freeze drying.

$$\text{CE of CIP (\% w/w)} = \frac{\text{Mass of CIP that formed CIP–ITZ nanoplex}}{\text{Initial mass of CIP added}} \times 100 \quad (1)$$

$$\text{CE of ITZ (\% w/w)} = \frac{\text{Mass of ITZ that formed CIP–ITZ nanoplex}}{\text{Initial mass of ITZ added}} \times 100 \quad (2)$$

$$\text{Yield (\% w/w)} = \frac{\text{Mass of CIP–ITZ nanoplex produced}}{\text{Initial masses of CIP,ITZ,DXT added}} \times 100 \quad (3)$$

2.2.4. Preparation of the binary mixture of CIP and ITZ nanoplexes

The binary mixture of CIP and ITZ nanoplexes was prepared by mixing aqueous suspensions of the CIP nanoplex and ITZ nanoplex at predetermined mass ratios that produced the same CIP and ITZ payloads as those exhibited by the dual-drug CIP-ITZ nanoplex prepared at $M_{ITZ/CIP}$ = 0.4, 0.8, and 1.6. The sample calculations for the mass ratios of the binary mixtures were presented in the Supplementary Materials. The single-drug CIP and ITZ nanoplexes were prepared and characterized following the methods presented in Cheow and Hadinoto [27] and Cheow, Kiew [29], respectively, hence they were not repeated here for brevity.

2.2.5. Dissolution rate under sink condition

The dissolution rates of CIP from the CIP-ITZ nanoplex suspension were investigated in triplicates under sink CIP condition at two pH values (i.e. 6.8 and 1.2) to simulate the varying pH environment of the gastrointestinal fluid. The dissolution medium used were (1) in 66 mM phosphate buffer solution (KH_2PO_4) adjusted to pH 6.8 by adding KOH and (2) in 0.2% (w/v) NaCl solution adjusted to pH 1.2 by adding HCl. Prior to the dissolution tests, the saturation solubility (C_{Sat}) of CIP in the buffer solutions at pH 6.8 and 1.2 were determined to be equal to 0.186 and 21.3 mg/mL, respectively, whereas C_{Sat} of ITZ at pH 6.8 and 1.2 were determined to be equal to 1.82 and 4.8 μg/mL, respectively. C_{Sat} was determined by incubating excess CIP (or ITZ) in the buffer solution in a shaking incubator at 37°C for 48 h, after which the solution was centrifuged to remove the undissolved drug. The amount of CIP (or ITZ) in the supernatant was then measured by HPLC as previously described.

Briefly, aqueous suspension of the CIP-ITZ nanoplex was added at $1/3\times C_{Sat}$ to a dialysis bag immersed in 20 mL buffer solution held at 37°C in a shaking incubator. Next, 1.0 mL aliquot was withdrawn and syringe filtered using 0.22-μm pore size at specific time points over a 4-h period, while 1.0 mL fresh buffer solution was added back to the vessel as replenishment. Afterwards, the aliquot was centrifuged at 14,000×g for 3 min and the amount of CIP in the supernatant was determined by HPLC as previously described. The CIP dissolution rates were also characterized for the native CIP, CIP nanoplex, and the binary mixture of CIP and ITZ nanoplexes.

The dissolution rate of ITZ from the CIP-ITZ nanoplex suspension was investigated in triplicates under sink ITZ condition at pH 1.2 in 0.1 M HCl supplemented with 0.7% (w/v) SDS. Herein the role of SDS was to increase the ITZ solubility in 0.1 M HCl as demonstrated previously by Thiry, Broze [37], thereby ITZ dissolution from the CIP-ITZ nanoplex could be effectively quantified. The dissolution rate of ITZ was characterized at $1/5\times C_{Sat}$, where C_{Sat} of ITZ in 0.1 M HCl with SDS was determined to be equal to 339 μg/mL, following the same procedures described in the above. Similar procedures as those carried out for determining the CIP dissolution rates were followed, but over a longer period of 144 h (6 days) due to the slower dissolution rate of ITZ. For comparison, the dissolution rates of ITZ from the native ITZ and the single-drug ITZ nanoplex were also characterized.

2.2.6. Supersaturation generation

The supersaturation generation of the CIP-ITZ nanoplex at pH 6.8 was characterized in triplicates by adding the CIP-ITZ nanoplex suspension in excess (i.e. at $10\times C_{Sat}$ of CIP) to 20 mL buffer solution held at 37°C in a shaking

incubator. Next, 300 µL aliquot was withdrawn and syringe filtered using 0.22-µm pore size at specific time points over 24 h. The aliquot was immediately diluted tenfold with fresh 50% (v/v) AA solution to prevent precipitation of CIP and ITZ from the supersaturated solution. The amounts of CIP and ITZ in the aliquot were then determined by HPLC as previously described. The supersaturation generation was characterized as the ratio of the supersaturated concentration of CIP (or ITZ) in the aliquot (C) to C_{Sat} of CIP (or ITZ). The effect of having pre-dissolved HPMC in the dissolution medium as a crystallization inhibitor was investigated at HPMC = 1 mg/mL. The supersaturation generation was also characterized for the CIP nanoplex and the binary mixture of CIP and ITZ nanoplexes.

3. Results and discussion

3.1. Co-complexation of CIP and ITZ with DXT

3.1.1. Preliminary study at $M_{ITZ/CIP}$ = 1.0

We began the investigation by examining the effect of the AA concentration used to dissolve CIP and ITZ on the physical characteristics of the particulate products of the co-complexation, because ITZ, despite being a weak base, was known to possess very low aqueous solubility in dilute acidic solutions (<< 10 µg/mL) [38]. Therefore, excess AA was needed to dissolve ITZ at a sufficiently high ITZ concentration for its formed complex with DXT to precipitate out of the solution. The AA concentration was investigated in the range of 50% to 80% (v/v), resulting in pH of the mixed (CIP + ITZ +DXT) solutions in the range of $1.6 \geq pH \geq 0.4$. On this note, CIP and ITZ at 5 mg/mL each ($M_{ITZ/CIP}$ = 1.0) were not fully soluble at AA < 50% (v/v).

The results showed that the size, zeta potential, and PDI of the co-complexation products, which were later to be verified in Section 3.2 as the dual-drug CIP-ITZ nanoplex, were not greatly affected by the variation in the AA concentration (Fig. 2A). Specifically, the size varied from 286 ± 18 nm with PDI = 0.331 ± 0.002 at 50% AA (pH 1.6) to 213 ± 14 nm with PDI = 0.338 ± 0.014 at 80% AA (pH 0.4). The zeta potential varied from -36 ± 1 mV to -33 ± 2 mV at 50% AA (pH 1.6) and 80% AA (pH 0.4), respectively, where the negative zeta potential was attributed to the presence of anionic DXT on the particle surface acting as stabilizers. The CIP and ITZ payloads were also minimally affected by the change in the AA concentration in which they remained constant at approximately 32% and 42% (w/w), respectively, resulting in a constant (CIP+ITZ) payload of ≈ 75% (w/w) (Fig. S1 of the Supplementary Materials).

In contrast, the drug utilization rate was found to decrease with increasing AA concentration, despite the higher degree of ionization of the basic drugs at lower pH (Fig. 2B). Specifically, the CEs of CIP and ITZ gradually decreased from 54 ± 1% and 90 ± 2% (w/w), respectively, at 50% AA (pH 1.6) to 22 ± 2% and 23 ± 2% (w/w), respectively, at 80% AA (pH 0.4). The lower CEs at higher AA concentrations was likely caused by the diminished anionic charge of DXT as the pH of the mixed solution dropped further below the pK_a of DXT, resulting in reduced electrostatic driving force for complexation with the cationic drugs. Not unexpectedly, the lower CEs translated to lower production yields, which decreased from 51 ± 1% (w/w) at 50% AA (pH 1.6) to 13 ± 2% (w/w) at 80% AA (pH 0.4) (Fig. 2B).

These results showed that while the physical characteristics of the dual-drug CIP-ITZ nanoplex were minimally affected by the AA concentration, their preparation efficiency worsened significantly at higher AA concentrations. Therefore, 50% AA (pH 1.6) was used in the subsequent studies in which the effects of $M_{ITZ/CIP}$ were examined. On this note, the control runs (i.e. without DXT) showed that no precipitation was observed upon mixing of the acidic drug solution with deionized water at equal volumes, which verified that the particulate products reported in the above was formed by complexation between the drugs and DXT.

3.1.2. Effects of $M_{ITZ/CIP}$

The effects of $M_{ITZ/CIP}$ in the feed solution were investigated in the range of 0.2 to 1.6 corresponding to $R_{drugs/DXT}$ in the range of 0.51 to 1.07, respectively. With the exception of the last run at $M_{ITZ/CIP}$ = 1.6 at which $R_{drugs/DXT}$ = 1.07, the study was performed at $R_{drugs/DXT}$ below unity. Therefore, excess charges of DXT were available for complexation with CIP and ITZ aimed at maximizing the drug utilization rate. As the study was conducted at constant CIP and DXT concentrations equal to 5.0 and 7.3 mg/mL, respectively, higher $M_{ITZ/CIP}$ values represented a preparation condition in which a larger amount of drugs was present in the feed solution to form complex with a fixed amount of DXT.

The results showed that the sizes of the CIP-ITZ nanoplexes prepared at $M_{ITZ/CIP} > 1.0$ were larger at ≈ 360-410 nm in comparison to those prepared at $M_{ITZ/CIP} \leq 1.0$ (≈ 160-280 nm) (Fig. 3A). The PDI, nevertheless, were comparable in the range of ≈ 0.327-0.363 at $M_{ITZ/CIP} \leq 1.0$ and ≈ 0.337-0.381 at $M_{ITZ/CIP} > 1.0$. On this note, the nanoscale size of the CIP-ITZ nanoplex had been verified by FESEM analysis using the CIP-ITZ nanoplex prepared at $M_{ITZ/CIP}$ = 1.0 as the representative sample (Fig. S2 of the Supplementary Materials). The zeta potentials also

varied in the range of -42 to -49 mV upon decreasing or increasing the $M_{ITZ/CIP}$ from 1.0 (Fig. 3A). The high zeta potentials observed across $M_{ITZ/CIP}$ values signified the good colloidal stability of the CIP-ITZ nanoplex.

More importantly, the results showed that the CIP and ITZ payloads of the CIP-ITZ nanoplex could be readily manipulated by varying $M_{ITZ/CIP}$ in the feed, where the CIP and ITZ payloads decreased and increased, respectively, with increasing $M_{ITZ/CIP}$ (Fig. 3B). Specifically, the CIP payload decreased as the amount of ITZ in the feed was increased from 62 ± 1% at $M_{ITZ/CIP}$ = 0.2 to 41 ± 2% and 31 ± 2% at $M_{ITZ/CIP}$ = 0.8 and 1.6, respectively. The ITZ payload correspondingly increased from 11 ± 1% at $M_{ITZ/CIP}$ = 0.2 to 36 ± 1 and 45 ± 2% at $M_{ITZ/CIP}$ = 0.8 and 1.6, respectively. It was worth noting that the total drug payload (i.e. CIP + ITZ) at different $M_{ITZ/CIP}$ remained constant at ≈ 75%, despite the variations in the individual drug payloads. Therefore, the increased presence of ITZ in the CIP-ITZ nanoplex occurred at the expense of the decreased presence of CIP, and vice versa.

The drug utilization rates were found to increase with increasing $M_{ITZ/CIP}$ for both CIP and ITZ, where the CEs of CIP and ITZ gradually increased from 53 ± 1% and 69 ± 3%, respectively, at $M_{ITZ/CIP}$ = 0.2, to 69 ± 1% and 96 ± 2%, respectively, at $M_{ITZ/CIP}$ = 1.6 (Fig. S3 of the Supplementary Materials). The fact that both CEs increased with increasing $M_{ITZ/CIP}$ indicated that larger amounts of CIP and ITZ were transformed to the nanoplex. The total drug payload, however, as we mentioned earlier, remained constant at ≈ 75% independent of $M_{ITZ/CIP}$. This suggested that the mass ratio of drugs to DXT in the CIP-ITZ nanoplex remained constant at different $M_{ITZ/CIP}$, despite the increase in the amount of drugs transformed to the nanoplex at higher $M_{ITZ/CIP}$.

The trends in the CE and total drug payload as a function of $M_{ITZ/CIP}$ thus suggested that a larger amount of DXT also underwent transformation to the nanoplex at higher $M_{ITZ/CIP}$. Not unexpectedly, the higher utilization rates of both the drugs and DXT at higher $M_{ITZ/CIP}$ resulted in higher overall production yields, which increased from 40 ± 2% at $M_{ITZ/CIP}$ = 0.2 to 79 ± 1% at $M_{ITZ/CIP}$ = 1.6. On this note, the increased participation of both the drugs and DXT to form the nanoplex at higher $M_{ITZ/CIP}$ provided an explanation for the aforementioned slightly larger size of the CIP-ITZ nanoplex prepared at $M_{ITZ/CIP} > 1.0$.

It was also noted that the CE of ITZ was found to be constantly higher (≈ 20-40% higher) than that of CIP in the range of $M_{ITZ/CIP}$ investigated (Fig. S3 of the Supplementary Materials). While the higher CE of ITZ at $M_{ITZ/CIP} > 1.0$ was not unexpected attributed to its larger presence in the feed solution, the higher CE of ITZ at $M_{ITZ/CIP} < 1.0$ signified the higher complexation propensity of ITZ. In this regard, the physical mechanisms of the drug-

polyelectrolyte complexation had been known to be predominantly cooperative [39], where the complex aggregates were primarily formed by hydrophobic interactions between the free drug molecules and the drug molecules that were already electrostatically bound to the polyelectrolyte chain. The significantly higher hydrophobicity of ITZ, where $LogP_{Octanol/Water}$ of ITZ was equal to 5.66 versus 0.28 for CIP [40], led to a higher degree of cooperative binding of the free ITZ, which in turn resulted in its higher CE.

3.1.3. FTIR and PXRD

The presence of both CIP and ITZ in the dual-drug CIP-ITZ nanoplex was verified by FTIR analysis using the nanoplex prepared at $M_{ITZ/CIP}$ = 1.0 as the representative sample. First, the presence of CIP was verified by the appearance of the peak at 1628 cm^{-1} in the FTIR spectrum of the CIP-ITZ nanoplex (Fig. 4A) corresponding to the C=O stretching of the pyridone functional group that was unique to CIP [41]. The same peak expectedly appeared in the FTIR spectrum of the single-drug CIP nanoplex. Compared to the FTIR spectrum of the native CIP, the pyridone peak in both the CIP nanoplex and the CIP-ITZ nanoplex was marginally shifted from 1618 cm^{-1} as a result of the protonation of CIP (Fig. 4A). The complexation between CIP and DXT was evident in the FTIR spectra of the CIP nanoplex and the CIP-ITZ nanoplex from the disappearance of the peak at 1595 cm^{-1}, which corresponded to the NH_2^+ bending of the protonated piperazine group of CIP, as a result of the electrostatic binding with the SO_3^- group of DXT.

Second, the presence of ITZ was verified by the appearance of the peaks at 1698 cm^{-1} in the FTIR spectrum of the CIP-ITZ nanoplex corresponding to the C=0 stretching of the triazole functional group that was unique to ITZ [42]. The presence of ITZ was also evident from the significant peak at 1510 cm^{-1} corresponding to C=C stretching of the two aromatic groups of ITZ. These two peaks expectedly appeared in the FTIR spectra of the native ITZ and single-drug ITZ nanoplex. The complexation between ITZ and DXT was evident in the FTIR spectra of the ITZ nanoplex and CIP-ITZ nanoplex from the disappearance of the peak at 1610 cm^{-1}, which corresponded to the $C=N^+$ stretching of the protonated triazole group of ITZ, due to the electrostatic binding with DXT.

Next, the amorphous state of the dual-drug CIP-ITZ nanoplex was verified by PXRD analysis using the nanoplex prepared at $M_{ITZ/CIP}$ = 1.0 as the representative sample. The PXRD pattern of the CIP-ITZ nanoplex showed the absence of sharp crystalline peaks, in contrast to the PXRD patterns of the native CIP and native ITZ,

and similar to the PXRD patterns of the single-drug CIP and ITZ nanoplexes (Fig. 4B). More specifically, broad amorphous halos were observed in the PXRD pattern of the CIP-ITZ nanoplexes.

3.2. Dual-drug CIP-ITZ nanoplex versus binary mixture of CIP and ITZ nanoplexes

3.2.1. Thermal behavior by DTA

In this section, we presented our experimental investigations to verify that the co-complexation products were indeed dual-drug CIP-ITZ nanoplex, and not binary mixture of the CIP nanoplex and ITZ nanoplex. The verification exercise was performed for the CIP-ITZ nanoplexes prepared at $M_{ITZ/CIP}$ = 0.4, 0.8, and 1.6, which were purposely selected because they possessed vastly different CIP and ITZ payloads. Specifically, the (CIP+ITZ) payloads of these nanoplexes were equal to approximately（50+25) %,（40+35) %, and（30+45) % at $M_{ITZ/CIP}$ = 0.4, 0.8, and 1.6, respectively. The CIP-ITZ nanoplexes were compared against binary mixtures of the single-drug CIP nanoplex and ITZ nanoplex exhibiting exactly the same (CIP+ITZ) payloads as the dual-drug nanoplexes.

The amorphous state of the CIP-ITZ nanoplexes was reaffirmed by DTA, where their DTA thermographs in Fig. 5A showed the absence of the endothermic melting point peaks at ≈ 265°C and 170°C, which were observed in the DTA thermographs of the crystalline native CIP and native ITZ, respectively. Instead, the CIP-ITZ nanoplexes exhibited distinct glass transitions events characteristic of an amorphous form at ≈ 210-220°C. Similar glass transition events were observed for the single-drug CIP nanoplex and ITZ nanoplex at ≈ 235°C and 200°C, respectively.

In contrast, the binary mixture of the CIP and ITZ nanoplexes exhibited significantly different DTA thermographs in which the aforementioned glass transition events at ≈ 210-220°C were noticeably absent (Fig. 5B). The DTA results thus served as the first evidence that the co-complexation products were not made up of binary mixtures of the CIP and ITZ nanoplexes, hence signified a successful preparation of the dual-drug CIP-ITZ nanoplex. On this note, the TGA showed that the nanoplexes (i.e. CIP-ITZ, CIP, and ITZ) had largely decomposed at temperatures above 240°C due to the DXT decomposition, therefore the DTA thermographs above 240°C were excluded from the analysis (Fig. S4 of the Supplementary Materials).

3.2.2. CIP dissolution characteristics

The successful preparation of the CIP-ITZ nanoplex was further verified by comparing the CIP dissolution characteristics of the nanoplexes prepared at $M_{ITZ/CIP}$ = 0.4, 0.8, and 1.6 with that of the binary mixtures under sink

condition. At pH 6.8, the CIP dissolution rate from the CIP-ITZ nanoplex was found to be diminished in comparison to the CIP dissolution from the CIP nanoplex or from the native CIP (Fig. 6A). Specifically, only approximately 50% of the CIP payload was dissolved from the CIP-ITZ nanoplex after 4 h, as opposed to nearly 100% and 70% dissolution for the CIP nanoplex and native CIP, respectively. The effect of the slower CIP dissolution rate exhibited by the CIP-ITZ nanoplex on its supersaturation generation capability was later investigated in Section 3.4.

The slower CIP dissolution rate of the CIP-ITZ nanoplex was also observed at pH 1.2, where less than ≈ 55% of the CIP payload was dissolved after 4 h, compared to more than ≈ 90% dissolution over the same period for both the CIP nanoplex and the native CIP (Fig. 6B). Furthermore, the CIP dissolution from the CIP-ITZ nanoplex at pH 1.2 was found to be dependent on the CIP payload, where the nanoplexes having the lower CIP payload (i.e. those that were prepared at $M_{ITZ/CIP}$ = 0.8 and 1.6) exhibited even slower dissolution rates in which less than ≈ 40% of the CIP payload was dissolved after 4 h. In other words, the increased presence of ITZ in the CIP-ITZ nanoplex resulted in slower CIP dissolution rates at pH 1.2.

In contrast, the binary mixtures of the CIP and ITZ nanoplexes exhibited very distinct CIP dissolution time-profiles compared to that of the CIP-ITZ nanoplex. At pH 6.8, the binary mixtures exhibited nearly 100% CIP dissolution after 4 h, which was highly comparable to the dissolution time-profile of the CIP nanoplex, hence signifying the absence of slower CIP dissolution rates in the binary mixtures (Fig. 7A). At pH 1.2, the binary mixtures exhibited more than ≈ 60% CIP dissolution after 4 h that was independent of the CIP payload, unlike the trend observed in the CIP-ITZ nanoplex (Fig. 7B). The highly distinct dissolution time-profiles between the CIP-ITZ nanoplex and the binary mixture served as the second evidence that the co-complexation products were indeed made up of the dual-drug nanoplex.

3.3. ITZ dissolution from the dual-drug CIP-ITZ nanoplex

The ITZ dissolution from the single-drug ITZ nanoplex at pH 1.2 was found to exhibit a sustained release profile, where 8 ± 2% and 53 ± 2% of the ITZ payload were released after 1 day and 6 days, respectively (Fig. S5 of the Supplementary Materials). Similar dissolution time-profiles were observed for the dual-drug CIP-ITZ nanoplex, where ≈ 8-17% and ≈ 67-75% (depending on $M_{ITZ/CIP}$) of the ITZ payload were released after 1 day and 6 days, respectively. In this regard, the variations in the ITZ dissolution between that observed in the ITZ nanoplex and the CIP-ITZ nanoplex were found to be statistically insignificant ($p \geq 0.05$). In contrast, owing to

its significantly higher C_{Sat} in the presence of SDS, the native ITZ exhibited a faster dissolution rate in which 69 ± 9% (w/w) of the ITZ payload was dissolved in 30 min and nearly 100% dissolution was achieved after 4 h.

The trend in the ITZ dissolution, where the native ITZ dissolved more rapidly than its nanoplex counterpart, was similar to the trend observed in the CIP dissolution at pH 1.2 in which the nanoplex exhibited slower CIP dissolution rates than the native CIP (Fig. 6B). Thus, the complexation of these basic drugs (i.e. CIP and ITZ) with DXT resulted in their slower dissolution rates in acidic condition compared to their native forms, as the protonatable groups of both CIP and ITZ were electrostatically bound with DXT. On this note, the significantly slower dissolution rate of ITZ compared to that of CIP from the CIP-ITZ nanoplex was not unexpected due to its significantly lower C_{Sat} at pH 1.2 compared to CIP (0.339 mg/mL versus 21.6 mg/mL, respectively).

3.4. Supersaturation generation of the dual-drug CIP-ITZ nanoplex

3.4.1. CIP and ITZ supersaturation generations

The supersaturation generation of the dual-drug CIP-ITZ nanoplex was first evaluated at pH 6.8 in the absence of HPMC as crystallization inhibitor in the dissolution medium. The results showed that the supersaturation generation of CIP by the dual-drug CIP-ITZ nanoplex was significantly diminished compared to that exhibited by the single-drug CIP nanoplex. Specifically, the single-drug CIP nanoplex exhibited the "spring-and-parachute" supersaturation time-profile that was characteristic of amorphous drug solids, where it achieved a maximum CIP supersaturation level of (8.3 ± 0.2)×C_{Sat} after 10 min ("spring"), which then gradually decreased to (1.9 ± 0.3)×C_{Sat} after 4 h due to the crystallization of the supersaturated solution ("parachute") (Fig. 8A). The supersaturation level eventually decreased to ≈ 1.0×C_{Sat} after 24 h (data not shown).

In contrast, the CIP-ITZ nanoplex prepared at $M_{ITZ/CIP}$ = 0.4 achieved a maximum CIP supersaturation level of only (2.9 ± 0.3)×C_{Sat} after 3 min, which then quickly decreased to ≈ 1.0×C_{Sat} after just 20 min (Fig. 8A). Even lower CIP supersaturation levels were generated by the CIP-ITZ nanoplexes prepared at $M_{ITZ/CIP}$ = 0.8 and 1.6, where the maximum CIP supersaturation levels did not reach higher than 1.1×$C_{Sat,}$ hence essentially signified the absence of supersaturation generation. These results thus showed that the CIP supersaturation generation of the CIP-ITZ nanoplex was increasingly diminished with increasing ITZ payload.

Despite its diminished CIP supersaturation generation, the CIP-ITZ nanoplex remained capable of generating high supersaturation levels for ITZ as reflected by the "spring-and-parachute" supersaturation time-profiles for ITZ. Specifically, the maximum ITZ supersaturation levels were equal to (184 ± 12)×C_{Sat}, (76 ± 14)×C_{Sat}, and (35 ± 5)×C_{Sat} for the nanoplexes prepared at $M_{ITZ/CIP}$ = 0.4, 0.8, and 1.6, respectively (Fig. 8B). These maximum supersaturation levels were rapidly achieved in just 1 min after which the supersaturation levels gradually decreased to ≈ 26×C_{Sat}, 8×C_{Sat}, and 5×C_{Sat} after 10 min, respectively, for the nanoplexes prepared at $M_{ITZ/CIP}$ = 0.4, 0.8, and 1.6. The supersaturation levels eventually settled at ≈ 3-4×C_{Sat} after 24 h (data not shown). On this note, the lower ITZ supersaturation levels exhibited by the CIP-ITZ nanoplexes having the higher ITZ payloads (i.e. those that were prepared at $M_{ITZ/CIP}$ = 0.8 and 1.6) were not unexpected, because they were attributed to the increased crystallization propensity of the supersaturated ITZ solution having a higher degree of ITZ supersaturation.

Significantly, the CIP supersaturation generation by the CIP-ITZ nanoplex remained lacking when the study was repeated in the presence of HPMC as the crystallization inhibitor in the dissolution medium. The results in Fig. S6 of the Supplementary Materials showed that the maximum CIP supersaturation levels never went above 1.1×C_{Sat}. These results hence indicated that the diminished CIP supersaturation generation exhibited by the CIP-ITZ nanoplex was not caused by rapid crystallization of the supersaturated CIP solution. Instead, the diminished CIP supersaturation generation was likely caused by factors that affected the amorphous solid phase of the nanoplex undergoing dissolution as we further elaborated in the next section.

3.4.2. Comparison with the binary mixtures

For comparison, the binary mixture of the CIP and ITZ nanoplexes having the same (CIP+ITZ) payload as the CIP-ITZ nanoplex prepared at $M_{ITZ/CIP}$ = 0.8 did not exhibit diminished supersaturation generations for both CIP and ITZ. The results in Fig. S7 of the Supplementary Materials showed that in the absence of crystallization-inhibiting HPMC in the dissolution medium, the binary mixture generated a maximum CIP supersaturation level of (7.4 ± 1.0)×C_{Sat} after 3 min, which then gradually decreased to (2.1 ± 0.2)×C_{Sat} after 4 h before it eventually settled at ≈ 1.0×C_{Sat} after 24 h (data not shown). For ITZ supersaturation, the binary mixture generated a maximum ITZ supersaturation level of (186 ± 13)×C_{Sat} after 3 min after which it gradually decreased to (9.4 ± 1.5)×C_{Sat} after 1 h before it settled at ≈ 4.0×C_{Sat} after 24 h (data not shown).

Significantly, the highly distinct supersaturation time-profiles exhibited by the binary mixture and the CIP-ITZ nanoplex prepared at $M_{ITZ/CIP}$ = 0.8 served as another evidence that the co-complexation products were indeed the dual-drug nanoplex. Moreover, the fact that the CIP supersaturation generation from the binary mixture was not diminished suggested that the presence of the supersaturated ITZ in the dissolution medium was not the cause either for the diminished CIP supersaturation generation exhibited by the CIP-ITZ nanoplex.

In this regard, a similar result in which the supersaturation generation of amorphous binary drug systems was significantly reduced compared to their single-drug counterparts had been reported previously for ASD and amorphous films [14]. The diminished supersaturation generation was explained to be caused by the decrease in the solubility of the metastable amorphous form of a given compound in the presence of a second compound due to the reduction in their chemical potentials [13, 14]. Therefore, the cause for the diminished CIP supersaturation generation from the dual-drug nanoplex was believed to be the lower solubility of the amorphous CIP in the presence of ITZ. The lower amorphous solubility of CIP led to the aforementioned slower CIP dissolution rates, which in turn increased the time-window for crystallization of the amorphous nanoplex by Ostwald ripening, resulting in the diminished supersaturation generation of CIP.

4. Conclusions

The present work successfully demonstrated a preparation of dual-drug amorphous nanoplex of CIP and ITZ via electrostatically driven co-complexation of the ionized drug molecules with oppositely charged DXT. First, we verified that the co-complexation products were the dual-drug CIP-ITZ nanoplex, instead of the binary mixture of the single-drug CIP and ITZ nanoplexes, by demonstrating their distinct (i) thermal behaviors, (ii) dissolution rates under sink condition, and (iii) supersaturation generation.

Second, the CIP-ITZ nanoplex exhibited size and zeta potential in the range of ≈ 160 to 410 nm (PDI ≈ 0.33-0.38) and ≈ -35 to -50 mV, respectively, depending on the preparation condition (i.e. pH and $M_{ITZ/CIP}$). The CIP-ITZ nanoplex exhibited a constant total (CIP+ITZ) payload of ≈ 75% (w/w) with the remaining 25% was made up of DXT, regardless of the preparation condition. The individual drug payload was, nevertheless, readily manipulated by varying $M_{ITZ/CIP}$ in the feed solution, resulting in CIP and ITZ payloads in the range of ≈ 60% to 30% and ≈ 15% to 45%, respectively, as $M_{ITZ/CIP}$ was increased from 0.2 to 1.6.

Third, in addition to its influence on the CIP-ITZ nanoplex's physical characteristics, $M_{ITZ/CIP}$ also affected the nanoplex's preparation efficiency, where higher $M_{ITZ/CIP}$ resulted in higher drug utilization rate and production yield. The CIP-ITZ nanoplex exhibited high preparation efficiency with drug utilization rates in the range of ≈ 50-70% for CIP and ≈ 70-100% for ITZ with overall production yield of ≈ 40-80% (w/w) depending on $M_{ITZ/CIP}$, where the higher ITZ utilization rates were attributed to its higher hydrophobicity compared to CIP.

Fourth, similar to other binary drug amorphous systems, the CIP-ITZ nanoplex exhibited highly diminished supersaturation generation, and consequently lower solubility enhancement capability, in comparison to the single-drug nanoplex, particularly for CIP. The decrease in the CIP supersaturation generation, which was likely caused by the slower CIP dissolution rates exhibited by the CIP-ITZ nanoplex, was intensified at higher ITZ payloads. The present results reaffirmed the finding that binary drug amorphous systems were prone to lower supersaturation generation in comparison to their single-drug counterpart. Investigations on whether a similar reduction in the supersaturation generation was also observed for dual-drug nanoplexes that were made up of different drugs are currently ongoing in our laboratory.

5. Acknowledgement

The authors would like to acknowledge the funding from GlaxoSmithKline (GSK) Singapore under their Green and Sustainable Manufacturing Trust Fund 2013 (PI: Kunn Hadinoto Ong)

6. Declaration of interests

The authors declare no conflict of interests

References

1. Ingersoll KS, Cohen J. The impact of medication regimen factors on adherence to chronic treatment: a review of literature. J Behav Med. 2008 Jun;31(3):213-224. doi: 10.1007/s10865-007-9147-y. PubMed PMID: WOS:000256090000004.

2. Bangalore S, Kamalakkannan G, Parkar S, et al. Fixed-dose combinations improve medication compliance: A meta-analysis. Am J Med. 2007 Aug;120(8):713-719. doi: 10.1016/j.amjmed.2006.08.033. PubMed PMID: WOS:000248694700026.

3. Pan F, Chernew ME, Fendrick AM. Impact of fixed-dose combination drugs on adherence to prescription medications. J Gen Intern Med. 2008 May;23(5):611-614. doi: 10.1007/s11606-008-0544-x. PubMed PMID: WOS:000255195300016.

4. Gupta AK, Arshad S, Poulter NR. Compliance, Safety, and Effectiveness of Fixed-Dose Combinations of Antihypertensive Agents A Meta-Analysis. Hypertension. 2010 Feb;55(2):399-407. doi: 10.1161/hypertensionaha.109.139816. PubMed PMID: WOS:000273802500035.

5. Hutchins V, Zhang B, Fleurence RL, et al. A systematic review of adherence, treatment satisfaction and costs, in fixed-dose combination regimens in type 2 diabetes. Curr Med Res Opin. 2011 Jun;27(6):1157-1168. doi: 10.1185/03007995.2011.570745. PubMed PMID: WOS:000290671800009.

6. Laurent C, Kouanfack C, Koulla-Shiro S, et al. Effectiveness and safety of a generic fixed-dose combination of nevirapine, stavudine, and lamivudine in HIV-1-infected adults in Cameroon: open-label multicentre trial. Lancet. 2004 Jul;364(9428):29-34. doi: 10.1016/s0140-6736(04)16586-0. PubMed PMID: WOS:000222392900028.

7. Monedero I, Caminero JA. Evidence for promoting fixed-dose combination drugs in tuberculosis treatment and control: a review. Int J Tuberc Lung Dis. 2011 Apr;15(4):433-439. doi: 10.5588/ijtld.09.0439. PubMed PMID: WOS:000288882300004.

8. Wedzicha JA, Dahl R, Buhl R, et al. Pooled safety analysis of the fixed-dose combination of indacaterol and glycopyrronium (QVA149), its monocomponents, and tiotropium versus placebo in COPD patients. Respir Med. 2014 Oct;108(10):1498-1507. doi: 10.1016/j.rmed.2014.07.011. PubMed PMID: WOS:000344425300012.

9. Kawabata Y, Wada K, Nakatani M, et al. Formulation design for poorly water-soluble drugs based on biopharmaceutics classification system: Basic approaches and practical applications. Int J Pharm. 2011 Nov;420(1):1-10. doi: 10.1016/j.ijpharm.2011.08.032. PubMed PMID: WOS:000296991500001.

10. Dengale SJ, Ranjan OP, Hussen SS, et al. Preparation and characterization of co-amorphous Ritonavir-Indomethacin systems by solvent evaporation technique: Improved dissolution behavior and physical stability without evidence of intermolecular interactions. Eur J Pharm Sci. 2014 Oct;62:57-64. doi: 10.1016/j.ejps.2014.05.015. PubMed PMID: WOS:000340301500008.

11. Fule R, Dhamecha D, Maniruzzaman M, et al. Development of hot melt co-formulated antimalarial solid dispersion system in fixed dose form (ARLUMELT): Evaluating amorphous state and in vivo performance. Int J Pharm. 2015 Dec;496(1):137-156. doi: 10.1016/j.ijpharm.2015.09.069. PubMed PMID: WOS:000365817100015.

12. Suresh K, Mannava MKC, Nangia A. A novel curcumin-artemisinin coamorphous solid: physical properties and pharmacokinetic profile. Rsc Advances. 2014;4(102):58357-58361. doi: 10.1039/c4ra11935e. PubMed PMID: WOS:000345460800034.

13. Trasi NS, Taylor LS. Thermodynamics of Highly Supersaturated Aqueous Solutions of Poorly Water-Soluble DrugsImpact of a Second Drug on the Solution Phase Behavior and Implications for Combination Products. J Pharm Sci. 2015 Aug;104(8):2583-2593. doi: 10.1002/jps.24528. PubMed PMID: WOS:000358009700021.

14. Trasi NS, Taylor LS. Dissolution performance of binary amorphous drug combinations-Impact of a second drug on the maximum achievable supersaturation. Int J Pharm. 2015 Dec;496(2):282-290. doi: 10.1016/j.ijpharm.2015.10.026. PubMed PMID: WOS:000367384700010.

15. Laitinen R, Lobmann K, Strachan CJ, et al. Emerging trends in the stabilization of amorphous drugs. Int J Pharm. 2013 Aug;453(1):65-79. doi: 10.1016/j.ijpharm.2012.04.066. PubMed PMID: WOS:000321741100008.

16. Chavan RB, Thipparaboina R, Kumar D, et al. Co amorphous systems: A product development perspective. Int J Pharm. 2016 Dec;515(1-2):403-415. doi: 10.1016/j.ijpharm.2016.10.043. PubMed PMID: WOS:000389150700040.

17. Alonzo D, Zhang G, Zhou D, et al. Understanding the Behavior of Amorphous Pharmaceutical Systems during Dissolution. Pharm Res. 2010;27(4):608-618. doi: 10.1007/s11095-009-0021-1.

18. Jog R, Burgess DJ. Pharmaceutical Amorphous Nanoparticles. J Pharm Sci. 2017 Jan;106(1):39-65. doi: 10.1016/j.xphs.2016.09.014. PubMed PMID: WOS:000393920500006.

19. Matteucci ME, Brettmann BK, Rogers TL, et al. Design of Potent Amorphous Drug Nanoparticles for Rapid Generation of Highly Supersaturated Media. Mol Pharmaceutics. 2007 2007/10/01;4(5):782-793. doi: 10.1021/mp0700211.

20. Dhumal RS, Biradar SV, Yamamura S, et al. Preparation of amorphous cefuroxime axetil nanoparticles by sonoprecipitation for enhancement of bioavailability. Eur J Pharm Biopharm. 2008 9//;70(1):109-115. doi: https://doi.org/10.1016/j.ejpb.2008.04.001.

21. Mou DS, Chen HB, Wan JL, et al. Potent dried drug nanosuspensions for oral bioavailability enhancement of poorly soluble drugs with pH-dependent solubility [Article]. Int J Pharm. 2011 Jul;413(1-2):237-244. doi: 10.1016/j.ijpharm.2011.04.034. PubMed PMID: WOS:000292583600029; English.

22. Miller MA, DiNunzio J, Matteucci ME, et al. Flocculated amorphous itraconazole nanoparticles for enhanced in vitro supersaturation and in vivo bioavailability [Article]. Drug Dev Ind Pharm. 2012 May;38(5):557-570. doi: 10.3109/03639045.2011.616513. PubMed PMID: WOS:000302164000005; English.

23. Lindfors L, Skantze P, Skantze U, et al. Amorphous drug nanosuspensions. 1. Inhibition of Ostwald ripening. Langmuir. 2006 Jan;22(3):906-910. doi: 10.1021/la0523661. PubMed PMID: WOS:000235068100014.

24. Arora A, Shafiq N, Jain S, et al. Development of Sustained Release "NanoFDC (Fixed Dose Combination)" for Hypertension - An Experimental Study. Plos One. 2015 Jun;10(6). doi: 10.1371/journal.pone.0128208. PubMed PMID: WOS:000355652200048.

25. Aryal S, Hu CMJ, Zhang LF. Combinatorial Drug Conjugation Enables Nanoparticle Dual-Drug Delivery. Small. 2010 Jul;6(13):1442-1448. doi: 10.1002/smll.201000631. PubMed PMID: WOS:000280219500012.

26. Huang WT, Larsson M, Lee YC, et al. Dual drug-loaded biofunctionalized amphiphilic chitosan nanoparticles: Enhanced synergy between cisplatin and demethoxycurcumin against multidrug-resistant stem-like lung cancer cells. Eur J Pharm Biopharm. 2016 Dec;109:165-173. doi: 10.1016/j.ejpb.2016.10.014. PubMed PMID: WOS:000390496500018.

27. Cheow WS, Hadinoto K. Self-assembled amorphous drug-polyelectrolyte nanoparticle complex with enhanced dissolution rate and saturation solubility. J Colloid Interface Sci. 2012 Feb;367:518-526. doi: 10.1016/j.jcis.2011.10.011. PubMed PMID: WOS:000299407500068.

28. Cheow WS, Hadinoto K. Green preparation of antibiotic nanoparticle complex as potential anti-biofilm therapeutics via self-assembly amphiphile-polyelectrolyte complexation with dextran sulfate. Colloids and Surfaces B-Biointerfaces. 2012 Apr;92:55-63. doi: 10.1016/j.colsurfb.2011.11.024. PubMed PMID: WOS:000300859000009.

29. Cheow WS, Kiew TY, Yang Y, et al. Amorphization Strategy Affects the Stability and Supersaturation Profile of Amorphous Drug Nanoparticles. Mol Pharmaceutics. 2014 May;11(5):1611-1620. doi: 10.1021/mp400788p. PubMed PMID: WOS:000335547500025.

30. Nguyen MH, Yu H, Dong BX, et al. A supersaturating delivery system of silibinin exhibiting high payload achieved by amorphous nano-complexation with chitosan. Eur J Pharm Sci. 2016 Jun;89:163-171. doi: 10.1016/j.ejps.2016.04.036. PubMed PMID: WOS:000376655600017.

31. Nguyen MH, Yu H, Kiew TY, et al. Cost-effective alternative to nano-encapsulation: Amorphous curcumin-chitosan nanoparticle complex exhibiting high payload and supersaturation generation. Eur J Pharm Biopharm. 2015 Oct;96:1-10. doi: 10.1016/j.ejpb.2015.07.007. PubMed PMID: WOS:000364881900001.

32. Yousefpour P, Atyabi F, Farahani EV, et al. Polyanionic carbohydrate doxorubicin-dextran nanocomplex as a delivery system for anticancer drugs: in vitro analysis and evaluations. Int J Nanomed. 2011;6:1487-1496. doi: 10.2147/ijn.s18535. PubMed PMID: WOS:000292593100001.

33. Dong BX, Hadinoto K. Amorphous nanoparticle complex of perphenazine and dextran sulfate as a new solubility enhancement strategy of antipsychotic perphenazine. Drug Dev Ind Pharm. 2017 Jun;43(6):996-1002. doi: 10.1080/03639045.2017.1287721. PubMed PMID: WOS:000399463600014.

34. Vitale RG, Afeltra J, de Hoog GS, et al. In vitro activity of amphotericin B and itraconazole in combination with flucytosine, sulfadiazine and quinolones against Exophiala spinifera. J Antimicrob Chemother. 2003 May;51(5):1297-1300. doi: 10.1093/jac/dkg218. PubMed PMID: WOS:000182629100031.

35. Skov M, Main KM, Sillesen IB, et al. Iatrogenic adrenal insufficiency as a side-effect of combined treatment of itraconazole and budesonide. Eur Respir J. 2002 Jul;20(1):127-133. doi: 10.1183/09031936.02.00248002. PubMed PMID: WOS:000177188600022.

36. Steinhart AH, Feagan BG, Wong CJ, et al. Combined budesonide and antibiotic therapy for active Crohn's disease: a randomized controlled trial. Gastroenterology. 2002 Jul;123(1):33-40. doi: 10.1053/gast.2002.34225. PubMed PMID: WOS:000176678600008.

37. Thiry J, Broze G, Pestieau A, et al. Investigation of a suitable in vitro dissolution test for itraconazole-based solid dispersions. Eur J Pharm Sci. 2016 Mar 31;85:94-105. doi: 10.1016/j.ejps.2016.02.002. PubMed PMID: WOS:000371996000011.

38. Prentice AG, Glasmacher A. Making sense of itraconazole pharmacokinetics. J Antimicrob Chemother. 2005 Sep;56:17-22. PubMed PMID: WOS:000231472400004.

39. Lei QL, Hadinoto K, Ni R. Complexation of Polyelectrolytes with Hydrophobic Drug Molecules in Salt-Free Solution: Theory and Simulations. Langmuir. 2017 Apr;33(15):3900-3909. doi: 10.1021/acs.langmuir.7b00526. PubMed PMID: WOS:000399860000039.

40. PubChem Compound Database (https://pubchem.ncbi.nlm.nih.gov/compound) by National Center for Biotechnology Information (Accessed 8 November 2017) [Internet]. 2017 [cited 8 November 2017].

41. Turel I, Bukovec P, Quiros M. Crystal structure of ciprofloxacin hexahydrate and its characterization. Int J Pharm. 1997 Jun;152(1):59-65. doi: 10.1016/s0378-5173(97)04913-2. PubMed PMID: WOS:A1997XG84200008.

42. Singh A, Bharati A, Frederiks P, et al. Effect of Compression on the Molecular Arrangement of Itraconazole-Soluplus Solid Dispersions: Induction of Liquid Crystals or Exacerbation of Phase Separation? Mol Pharmaceutics. 2016 Jun;13(6):1879-1893. doi: 10.1021/acs.molpharmaceut.000046. PubMed PMID: WOS:000377424600013.

Figure captions

Fig. 1 Schematic of the electrostatically driven co-complexation of cationic CIP and ITZ molecules with oppositely charged DXT in which two plausible outcomes were investigated, i.e. (1) the formation of binary mixture of CIP nanoplex and ITZ nanoplex, or (2) the formation of dual-drug CIP-ITZ nanoplex

Fig. 2 Effects of AA concentration on the (A) size, zeta potential; (B) CE, yield of the CIP-ITZ nanoplex

Fig. 3 Effects of $M_{ITZ/CIP}$ on the (A) size, zeta potential; (B) CIP and ITZ payloads of the CIP-ITZ nanoplex

Fig. 4 (A) FTIR spectra and (B) PXRD patterns of the CIP-ITZ nanoplex, CIP nanoplex, ITZ nanoplex, native CIP, native ITZ, and DXT using the CIP-ITZ nanoplexes prepared at $M_{ITZ/CIP}$ = 1.0 as the representative sample

Fig. 5 DTA thermographs of (A) the CIP-ITZ nanoplex, CIP nanoplex, ITZ nanoplex, native CIP, native ITZ, and DXT; (B) DTA thermographs of the binary mixture of CIP and ITZ nanoplexes that had the same CIP and ITZ payloads as the CIP-ITZ nanoplexes prepared at $M_{ITZ/CIP}$ = 0.4, 0.8, and 1.6.

Fig. 6 CIP dissolution rates from the CIP nanoplex and from the CIP-ITZ nanoplexes prepared at $M_{ITZ/CIP}$ = 0.4, 0.8, and 1.6 in buffer solutions at (A) pH 6.8 and (B) pH 1.2

Fig. 7 CIP dissolution rates from the binary mixtures of CIP and ITZ nanoplexes that had the same CIP and ITZ payloads as the CIP-ITZ nanoplexes prepared at $M_{ITZ/CIP}$ = 0.4, 0.8, and 1.6 in buffer solutions at (A) pH 6.8 and (B) pH 1.2.

Fig. 8 (A) CIP and (B) ITZ supersaturation time-profiles generated by the CIP-ITZ nanoplex prepared at $M_{ITZ/CIP}$ = 0.8 in the absence of HPMC in the dissolution medium (pH 6.8)

Fig. 1

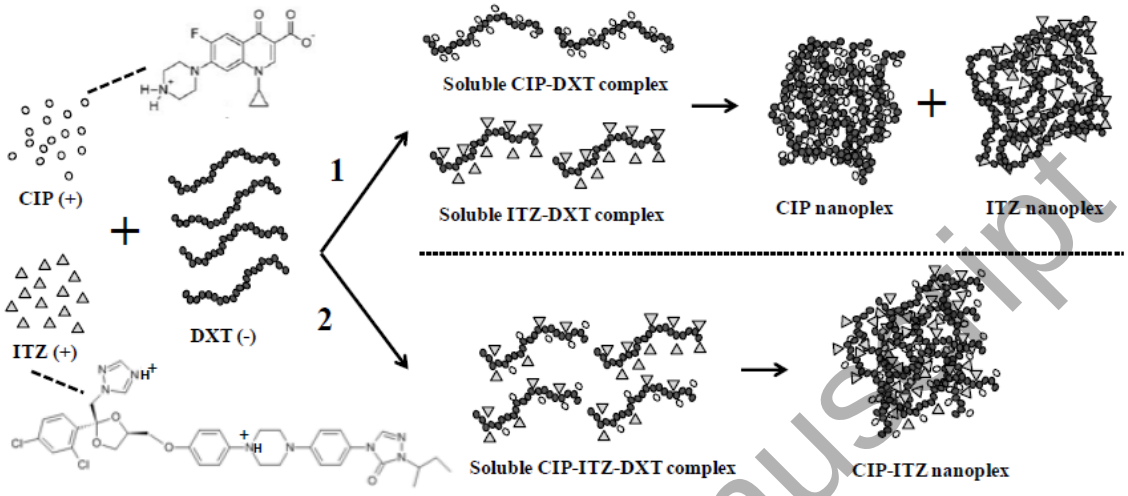

Fig. 2

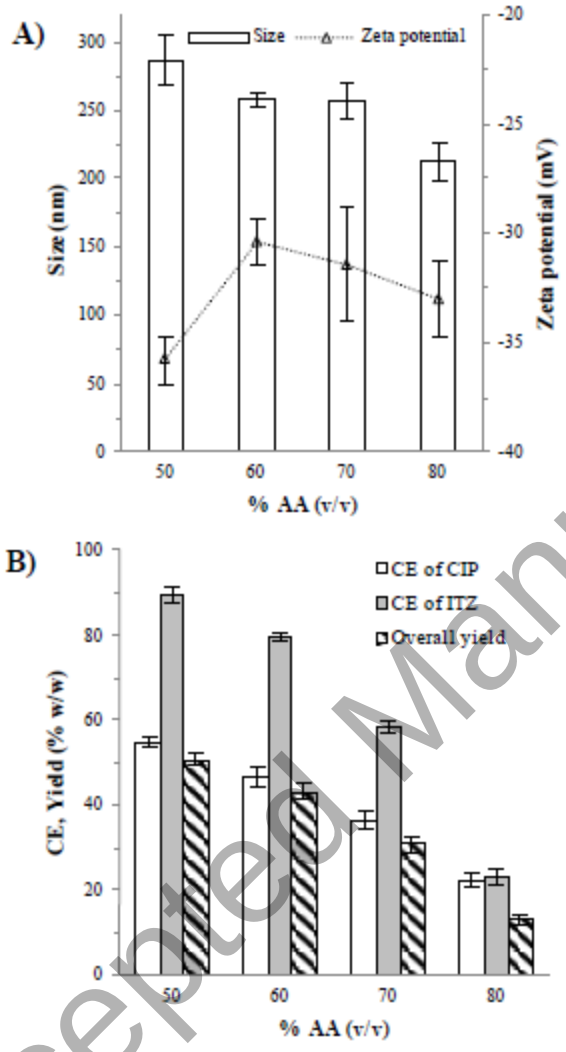

Fig. 3

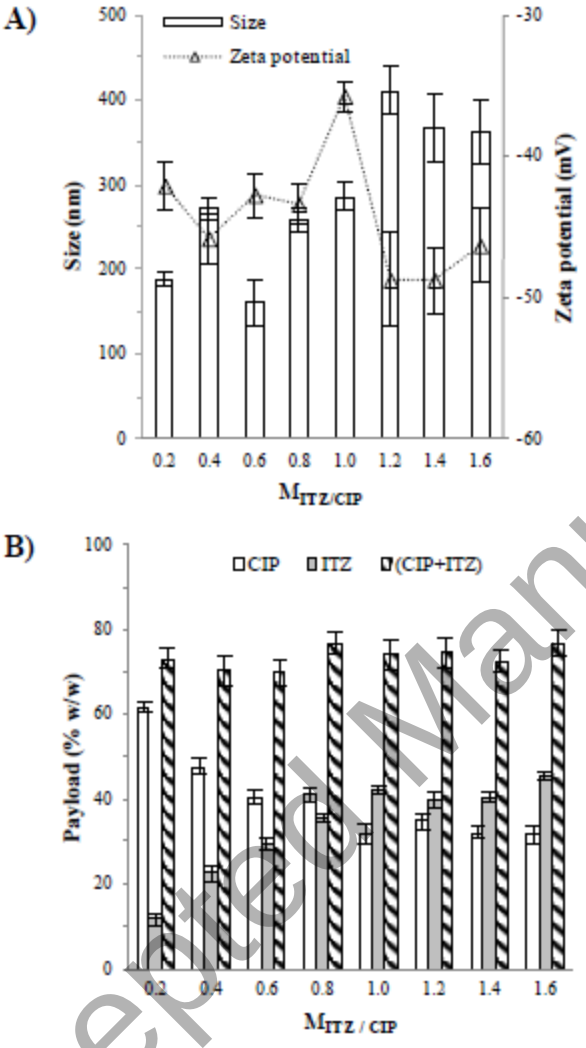

Fig. 4

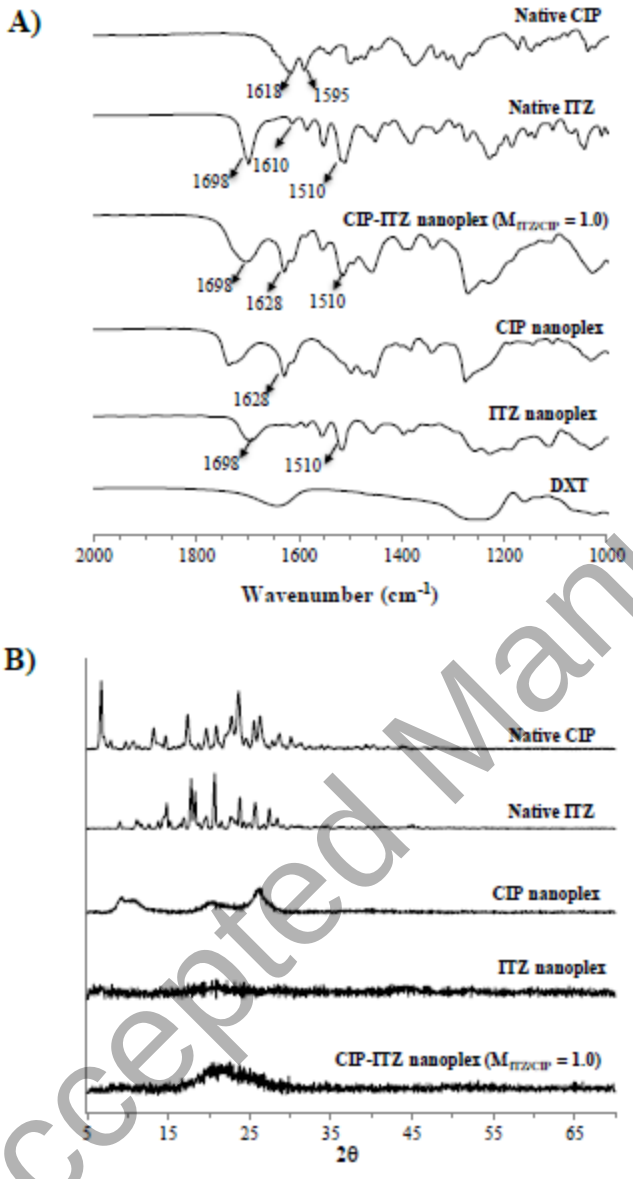

Fig. 5

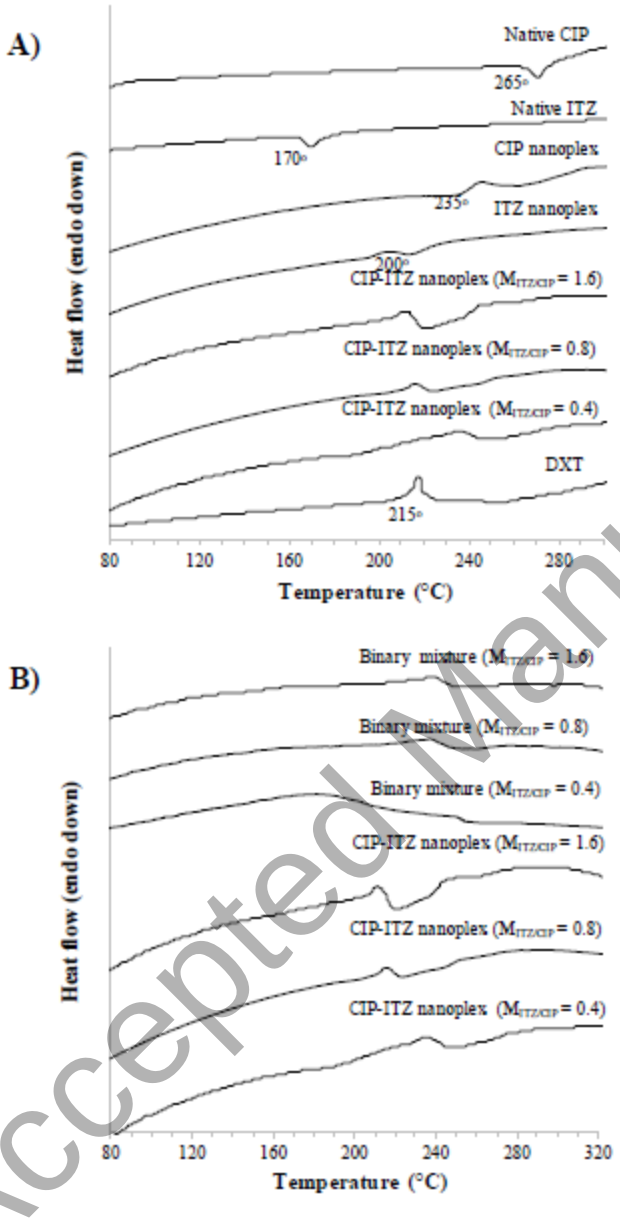

Fig. 6

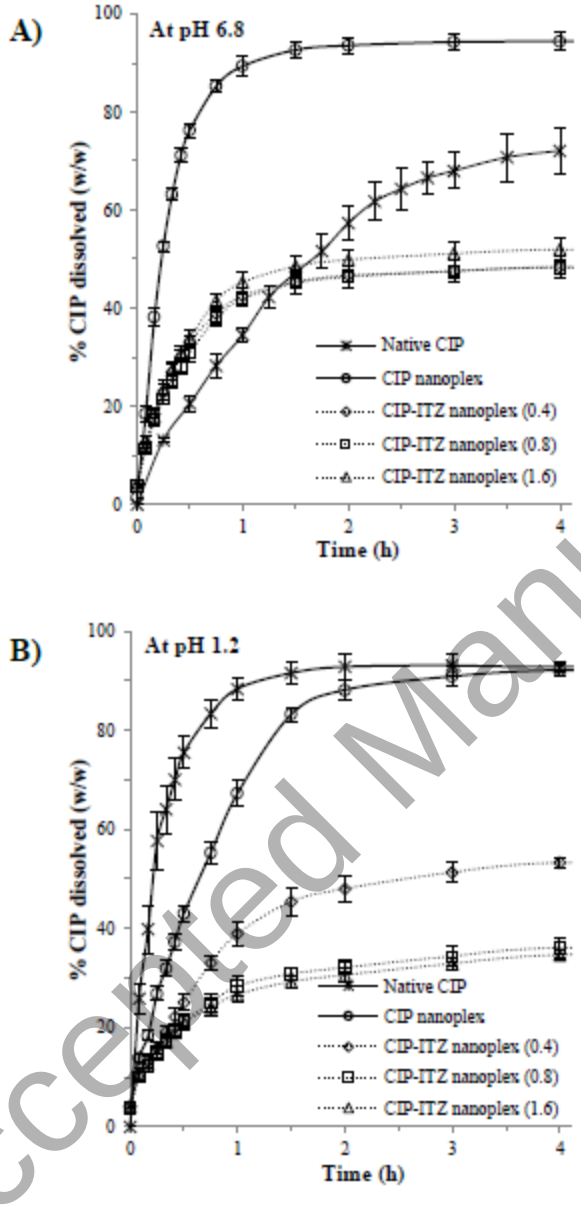

Fig. 7

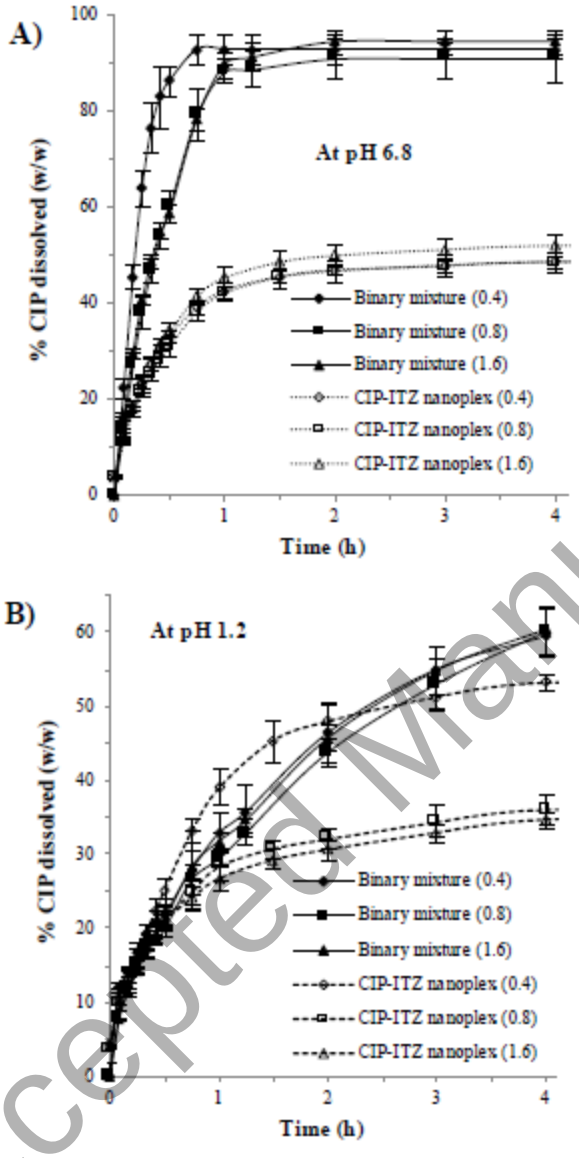

Fig. 8